Title

Patterning Technique for Generating Arbitrary Anisotropic Impedance Surfaces

Journal

IEEE Transactions on Antennas and Propagation, 64(11)

ISSN

0018-926X

Authors

Lee, Jiyeon

Sievenpiper, Daniel F

Publication Date

2016-11-01

DOI

10.1109/tap.2016.2608935

Peer reviewed

Patterning Technique for Generating Arbitrary Anisotropic Impedance Surfaces

Jiyeon Lee, *Student Member, IEEE*, and Daniel F. Sievenpiper, *Fellow, IEEE*

***Abstract*— Anisotropic impedance surfaces have been demonstrated to be useful for a variety of applications ranging from antennas, to surface wave guiding, to control of scattering. To increase their anisotropy requires elongated unit cells which have reduced symmetry and thus are not easily arranged into arbitrary patterns. We discuss the limitations of existing patterning techniques, and explore options for generating anisotropic impedance surfaces with arbitrary spatial variation. We present an approach that allows a wide range of anisotropic impedance profiles, based on a point-shifting method combined with a Voronoi cell generation technique. This approach can be used to produce patterns which include highly elongated cells with varying orientation, and cells which can smoothly transition between square, rectangular, hexagonal, and other shapes with a wide range of aspect ratios. We demonstrate a practical implementation of this technique which allows us to define gaps between the cells to generate impedance surfaces, and we use it to implement a simple example of a structure which requires smoothly varying impedance, in the form of a planar Luneberg lens. Simulations of the lens are verified by measurements, validating our pattern generation technique.**

***Index Terms*— Anisotropic surface, artificial material, luneberg lens, metasurface, patterning, surface impedance, surface waves.**

I. Introduction

An ARTIFICIAL impedance surface is a metasurface which is fabricated with periodic metallic patches on a grounded dielectric substrate. It has been used for various applications including control of surface waves [1], [2], scattering [3], conformal antennas [4], and waveguides [5]–[7]. Their electromagnetic properties are defined by the thickness of the substrate, and the capacitance between patches, which together determine the effective surface impedance. Varying the cell size and shape allows the impedance to be controlled. Vertical conducting vias are sometimes also used, but they are only necessary if very high impedance values are needed, or to completely block surface waves [8]. Initial impedance surfaces consisted of simple square or hexagonal cells. However, reducing the symmetry of the cells allows the surface to have anisotropic impedance properties. This is important for applications such as surface wave cloaking, interference reduction between RF apertures, control over polarization, and conversion between transverse magnetic (TM) and transverse electric surface waves.

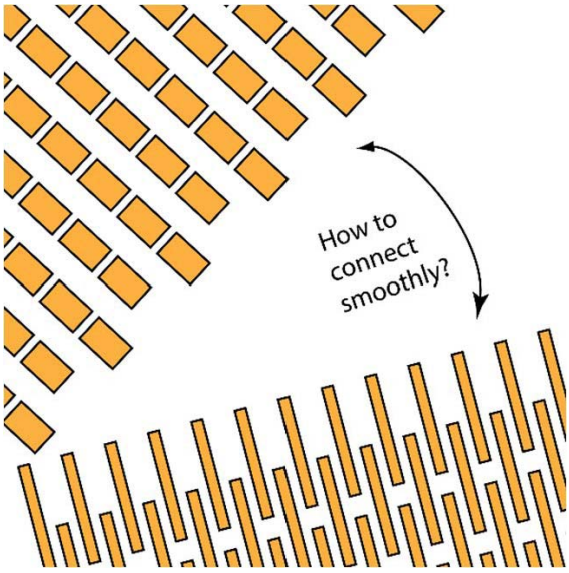

Fig. 1. Primary challenge in current artificial impedance surface research is how to pattern impedance surfaces to produce arbitrary impedance profiles when the surface is highly anisotropic or has impedance that varies dramatically with position.

Until recently it was not possible to create smoothly varying, highly anisotropic impedance functions because of the difficulty of patterning regions in which the cell size, shape, and orientation varied. Illustrated in Fig. 1, there was no available method to smoothly connect these regions with different impedance values and with different primary directions, aside from drawing each cell manually, which is impractical. The challenge is how to pattern elongated unit cells which allow high anisotropy, but to also create arbitrary and smoothly varying impedance patterns. All previous work in this area used discrete regions of different impedance values or directions [3], [5].

Several existing approaches to patterning anisotropic surfaces can be found in the literature, and examples are shown in Fig. 2. The first anisotropic impedance surface [9] shown in Fig. 2(a) used slices in a lattice of square patches, that are rotated to an arbitrary angle. For example, if the slices are oriented along the y-direction, the structure has twice as many capacitive gaps along x as along y, due to the extra capacitance of the slice. Thus, the maximum anisotropy of

Manuscript received August 3, 2015; revised April 24, 2016; accepted July 6, 2016. Date of publication September 13, 2016; date of current version October 27, 2016. This work was supported by the Air Force Office of Scientific Research under Grant FA9550-16-1-0093.

The authors are with the University of California at San Diego, La Jolla, CA 92093-0407 USA (e-mail: y0l001@ucsd.edu).

Color versions of one or more of the figures in this paper are available online at http://ieeexplore.ieee.org.

Digital Object Identifier 10.1109/TAP.2016.2608935

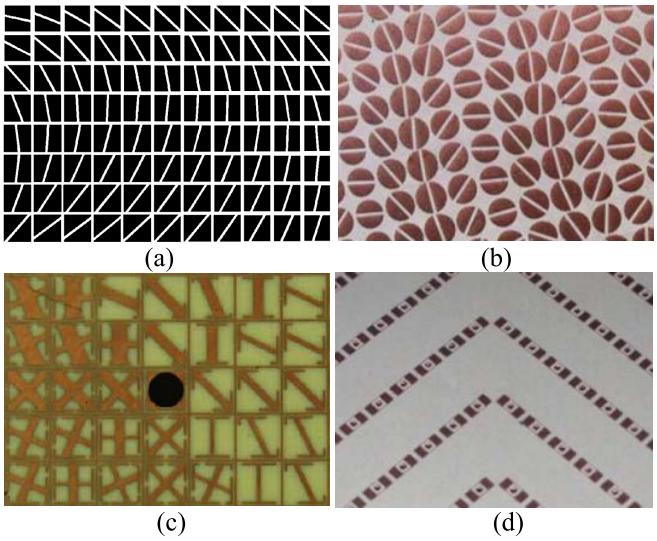

Fig. 2. Examples of anisotropic surfaces include (a) square or (b) circular patches with slices rotated to an arbitrary angle, or (c) other patterns confined to a square lattice, as well as (d) lower symmetry cells that cannot be arranged into arbitrary patterns.

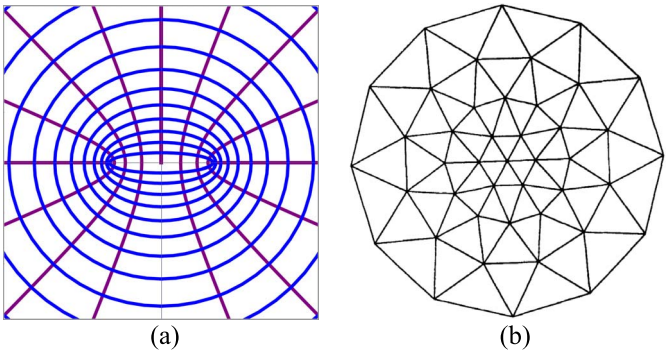

Fig. 3. Other possible approaches to patterning smoothly varying impedance surfaces include (a) conformal mapping and (b) mesh generation techniques. Neither of these produces anisotropic impedance surfaces with the properties needed for applications.

such a structure is roughly 2:1. A structure based on circular patches [10] shown in Fig. 2(b) is similar and suffers from the same limitation. In Fig. 2(c), the structure [11] involved capacitive regions connected by inductive bars that are rotated to arbitrary angles. If the angle of rotation varies too rapidly between adjacent cells, the capacitive regions do not line up. It is also limited by the use of a square grid. Fig. 2(d) shows that elongated unit cells [3] can provide a high range of anisotropy, however, these require a rectangular grid. Any design that reduces symmetry of the lattice itself cannot be patterned to include an arbitrarily varying angle of anisotropy.

Other approaches exist for creating smoothly varying and arbitrary geometrical patterns, however, they do not have the required properties for artificial impedance surfaces. Conformal mapping [12], [13], illustrated in Fig. 3(a) is one option which is commonly used for defining effective permeability or permittivity in transformation optics applications [14]. It could potentially be applied to generating cells for impedance surfaces. However, it has the limitation that the cell size, shape,

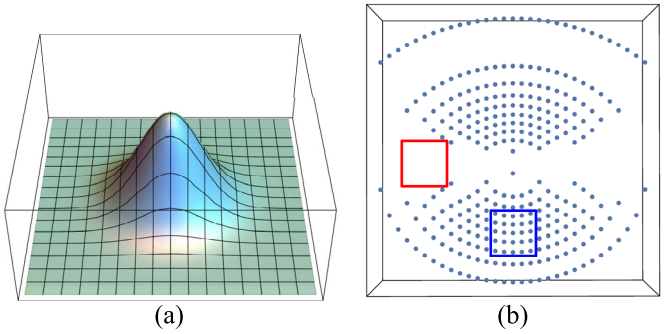

Fig. 4. Another method called the point density approach involves choosing points with a density based on (a) function whose slope represents the local impedance function. (b) Resulting set of points represents the centers of the cells, but their location depends on the path over which one traverses the original function. Discrepancies are indicated at the red and blue squares.

and orientation would be highly dependent on the divergence of the local impedance function. As illustrated in Fig. 3(a), as the lines diverge, the cells get larger in the direction perpendicular to the lines, which also sets their orientation. This is true of any patterning technique that relies on defining cell boundaries by continuous lines. Thus, while conformal mapping is useful for determining impedance profiles to achieve certain functional properties, it is not appropriate for defining the unit cells to create those impedance profiles. Our approach to be described below provides more freedom in defining impedance surfaces that have dramatic changes in impedance over short distances.

Mesh generation techniques have been developed for physical modeling codes for many years, and typically produce patterns such as shown in Fig. 3(b) [15]. These could potentially be applied to patterning impedance surfaces as well. However, they are generally designed to provide a specific average cell density, without concern for the details of the cell shape. For impedance surfaces the cell shape is very important for determining the anisotropic impedance values.

We explored another option that we called the point density method as illustrated in Fig. 4. The idea is to start with a function in Fig. 4(a), the slope of which represents the local impedance. By traversing that function, we can define a point which represents the center of a unit cell each time the function reaches an integer value, or at some other uniform interval of z-axis and another axis among x- and y-axis. The problem with this approach is that it is highly dependent on the path over which one traverses the function. As shown in Fig. 4(b) it does not produce a unique set of unit cells. This is one example of many path-dependent approaches that we determined were unable to produce patterns which required properties for impedance surfaces.

In this paper, we introduce a new patterning technique based on a point shifting method with cells defined using the Voronoi technique. In Section II, we describe the details of how the method is implemented, and illustrate the range of patterns that can be created. In Section III, we demonstrate that it can produce useful structures by building an example of a smoothly varying impedance function, in the form of a well-known planar Luneburg lens [16]–[18]. Measurements show

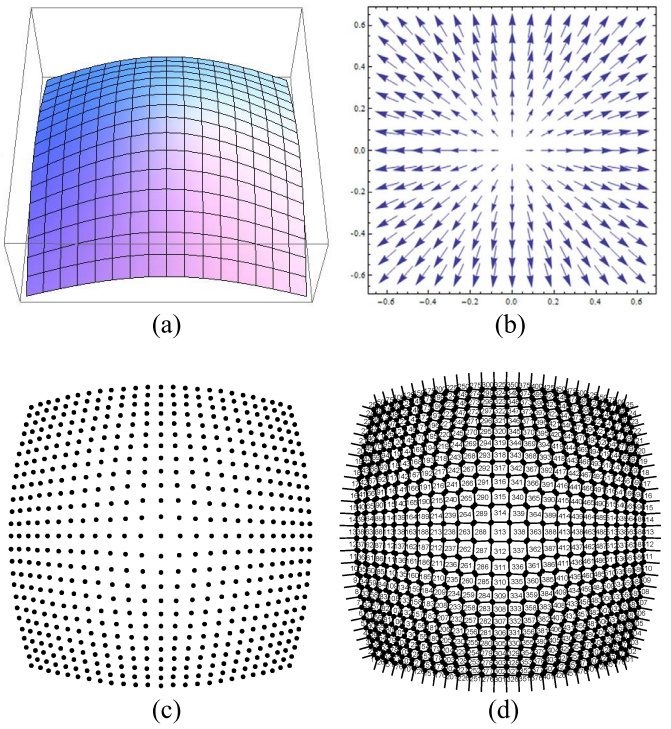

Fig. 5. (a) Starting function with a local maximum. (b) Set of gradient vectors which define the movement of points. (c) Final set of points. (d) Unit cells generated by the Voronoi method.

that the field profile matches the simulations, verifying that this method produces the intended impedance profile.

II. Patterning Process

We developed a patterning technique to produce arbitrary anisotropic surfaces which we call the point shifting method. For our patterning method, we define a function that is related to the desired surface impedance in each direction, which is related to the cell size in that direction. We currently choose this starting function based on knowledge of the desired cell profile. We then define a uniform grid of points with a period equal to the average cell size. Next, we shift each point in proportion to the gradient vector of the starting function. This is illustrated in Fig. 5(a) which shows a function with a local maximum, and in Fig. 5(b) which shows each point moving with a direction and magnitude that is in proportion to its gradient vector. The result is that the distance between neighboring points is expanded near local maxima, and compressed near local minima. In regions with constant slope, the points all shift by the same amount, resulting in no change in the distance between them. Fig. 5(c) shows the final lattice of points for this example. Anisotropic cells are created by compressing or stretching the distance between points in one direction relative to the other. Thus, the anisotropy in the final lattice of points is defined by the anisotropy of the curvature in the starting function. The cells are generated from the grid of points using a Voronoi technique, as shown in Fig. 5(d).

A Voronoi diagram is an approach for dividing regions based on a set of points and the Euclidean distance between those points [19]. To create a 2-D Voronoi diagram, one draws

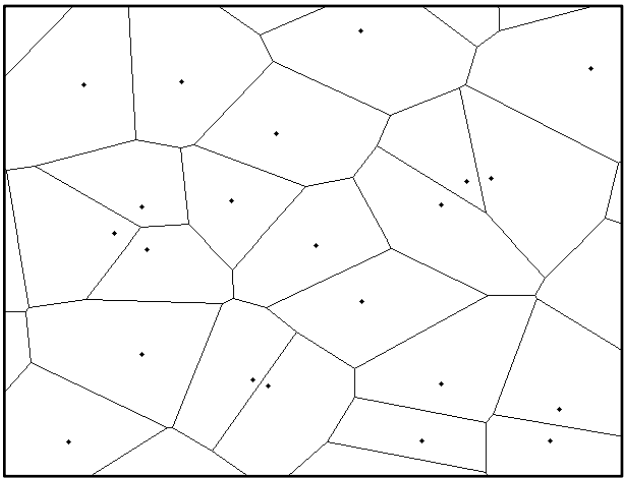

Fig. 6. Voronoi diagram for a random set of points. Each cell is defined as the region that is closer to each point than to any of its neighbors.

a midline between each pair of neighboring points, which is perpendicular to a line drawn from one point to the other. For each point, the collection of midlines to each of its neighbors defines the cell associated with that point. This is the same method used to define Brillouin zones for crystals [20]. Fig. 6 shows an example of Voronoi diagram for a random set of points. The Voronoi function is available in codes such as Mathematica and MATLAB.

The relationship between the properties of the Voronoi cells and the surface impedance is defined by the details of the cell geometry. For a fixed substrate thickness and dielectric constant, higher impedance can be obtained using larger cells, or smaller gaps [1]. The surface impedance is defined as the ratio of the tangential electric and magnetic fields. It can be direction-dependent in the case of anisotropic surfaces, and the impedance along a particular direction is primarily determined by the length and gap width in that direction [5]. Varying only the gap width limits the range of available impedance values, but allowing the cell size to vary provides a wider design space. Furthermore, more complex anisotropic structures cannot be designed without either elongated unit cells (which cannot be patterned into arbitrary functions with any existing techniques) or more complicated cell geometries [11]. For this reason, we are developing a patterning technique that allows for continuous variation of cell size, shape, and orientation.

After an array of cells is patterned on the *xy* plane, a gap is required between neighboring cells to define an artificial impedance surface. The process of generating a constant gap width starts with calculating the distance between the center point and one side of the cell. Each cell is defined by its center point and vertices. We define a line connecting each pair of vertices, as shown in Fig. 7(a), and then calculate the length of the segment running from the center point and perpendicular to this line, as shown in Fig. 7(b). The next step is calculating the ratio between the distance calculated in Fig. 7(b) and half of the assigned gap which is shown in Fig. 7(c) as a blue line. After the ratio is obtained, it can be used to calculate the coordinates of new vertexes for each cell. Each vertex is moved

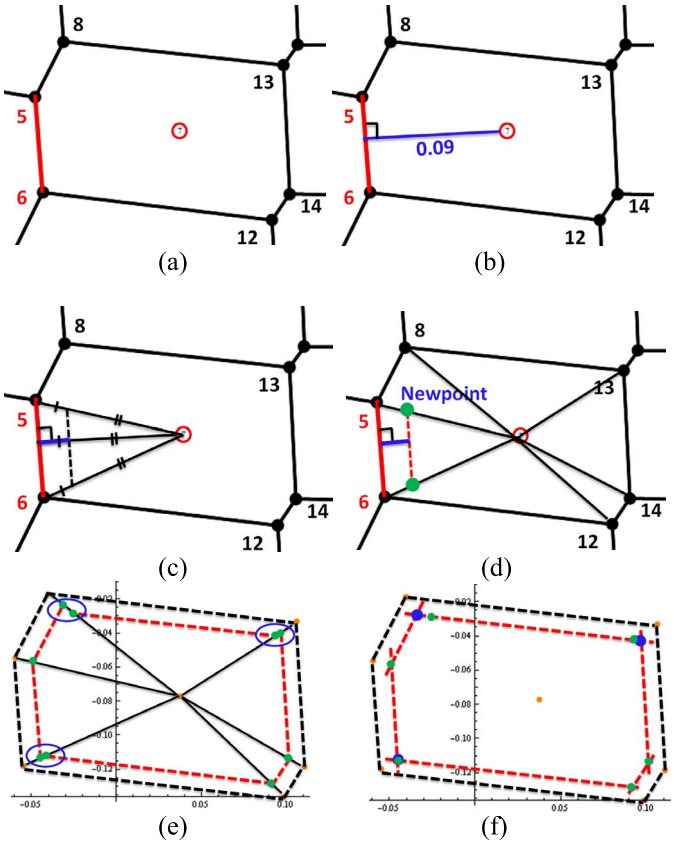

Fig. 7. (a) Cell defined by a center point and vertices. (b) Segment shown in blue from the center point to a line connecting two vertices shown in red. (c) Half the intended gap width is shown in blue. (d) Vertices are moved toward the center point by a distance that is proportional to the gap width. (e) Errors are introduced due to the varying angles between adjacent sides. (f) Errors are corrected by placing new vertices at the intersections between lines defined by each side. The final cell has constant gap width.

toward the center of the cell by a distance that is defined by the ratio calculated above, as shown in Fig. 7(d). This process is used to create each new side of the cell, as shown in Fig. 7(e). However, the varying angles between sides create errors in the definition of the new cell which must be corrected. The solution is to take the intersections of lines created from the new sides to generate corrected vertices, shown as blue dots in Fig. 7(f). These new points complete the new cell with a constant gap width. This process is repeated for all cells in the array to generate a file which defines the metallic pattern that forms the artificial impedance surface.

The cells are generally designed to be electrically small at the frequency of interest so that they can be considered in the effective medium limit, and the surface can be described as an effective impedance boundary. Refraction or reflection [1] does not occur at the individual cell boundaries, but rather due to large-scale variation in the effective surface impedance.

Fig. 8 shows the range of properties that can be created using our point shifting method. This approach enables not only smoothly varying impedance functions, but also varying cells with arbitrary shapes, sizes, and direction of anisotropy as a function of position. The patterns in Fig. 8 were generated by starting function with a square grid. However, we have

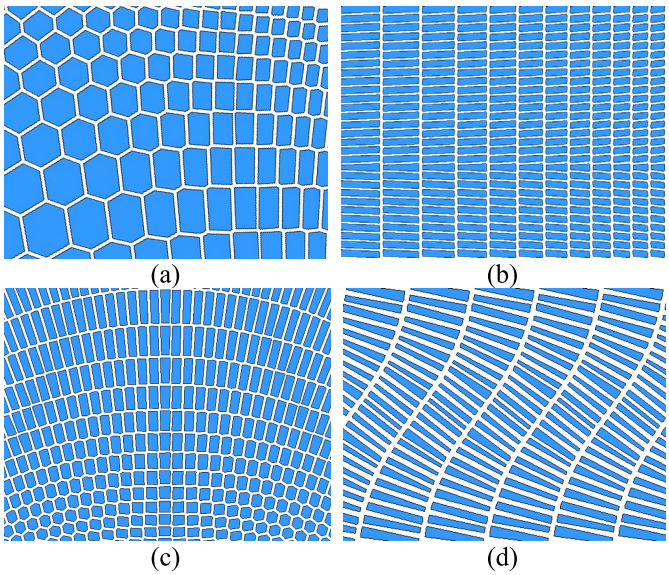

Fig. 8. Examples of various patterns that can be produced by this technique. (a) Varying cell shape. (b) Gradient of impedance. (c) Varying orientation. (d) Extreme variation with high anisotropy.

also developed code to start with a triangular grid, which can produce similar results, allowing a wider range of possible patterns. After having demonstrated the range of properties that are achievable with this method we now use it to create a simple example of a structure which requires a smoothly varying impedance profile, in the form of a planner Luneburg lens. We should note that our method is applicable to general tensor impedance surfaces having a wide range of properties including anisotropy, as illustrated in Fig. 8. However, since canonical anisotropic impedance surface problems are not widely known, for the purpose of demonstrating and validating our patterning method we choose a common problem with a well-defined solution that requires a smoothly varying surface impedance. For this reason, we have selected a planar Luneburg lens design as an example.

III. Luneburg Lens Patterning

A Luneburg lens is a spherically symmetric gradient-index lens [16]. The refractive index n of the lens follows the function:

$$\mathrm{n} = \sqrt{\varepsilon_r} = \sqrt{2 - \left(\frac{r}{R}\right)^2} \tag{1}$$

where r is the radial distance from the center of the lens and R is the radius of the lens. The index n falls from $\sqrt{2}$ to 1 from the center to the edge. It has also been demonstrated in planar form using impedance surfaces [21], [22]. As an example of a practical application of our point shifting method, we generate an inhomogeneous impedance surface with the Luneburg lens profile. We then simulate and measure it to verify that this approach can produce the intended impedance pattern.

A. Patch Simulation Results and Impedance Data

The patterned Luneburg lens consists of patches which set the surface impedance. Therefore we first analyze the

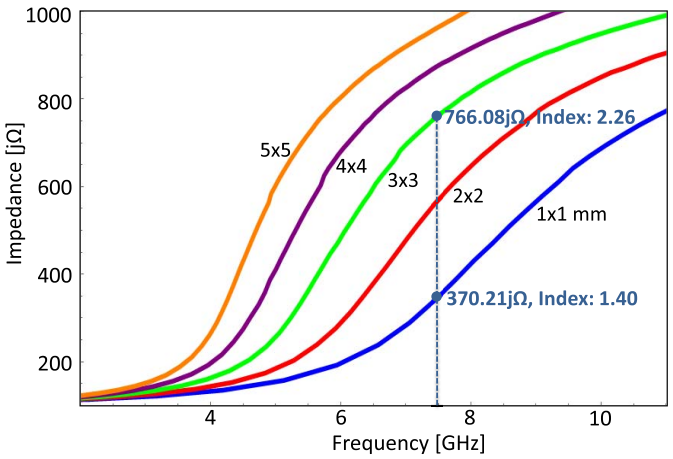

Fig. 9. Simulated impedance versus frequency for various sizes of square unit cells on 2.5 mm Rogers 6010 with 0.25 mm gaps. The indicated impedance range of 766.08 to 370.21 jΩ corresponds to an index ratio of 1.6:1.

impedance as a function of cell geometry to determine the appropriate range of cell sizes for a given substrate and thickness. Assuming grounded 2.5 mm thick Rogers 6010 substrate ($\varepsilon_r = 10.2$), we studied cells ranging in size from 1 to 5 mm, shown in Fig. 9. The gap was 0.25 mm for each case. Although the patches will have various shapes, we studied square patches as a compromise that is representative of a typical patch. We have previously shown that for anisotropic surfaces with rectangular unit cells, the impedance along one direction is independent of the cell size in the orthogonal direction [1], so simulations of square cells provide an understanding of the behavior of rectangular cells as well.

The unit cell structure was simulated in the eigenmode solver in Ansys HFSS version 15.0.3 (a full-wave, commercial software package). The surface impedance for TM waves was calculated as

$$Z_{\mathrm{TM}} = Z_0\sqrt{1-\left(\frac{k_{\mathrm{TM}}c}{\omega}\right)^2} \tag{2}$$

based on the dispersion results of the unit cell [8], [23].

Fig. 9 shows the frequency-dependent surface impedance plot of unit cells from 1×1 mm to 5×5 mm. In this plot TM surface impedance can be translated to the index so that the analysis allows us to find an appropriate range of cells which follows the index profile of a Luneburg lens. The effective TM index for surface waves is defined as [24]

$$n_s = \sqrt{1-\left(\frac{Z_{\mathrm{TM}}}{Z_0}\right)^2}. \tag{3}$$

According to the simulation results we can find appropriate cell sizes which support the surface impedance range for the Luneburg lens index at around 7–8.5 GHz. Fig. 9 shows the result at 7.5 GHz which is selected as the operating frequency of our Luneburg lens pattern. In order to approximate the Luneburg lens profile, we choose a range of cells varying from 1 to 3 mm, which corresponds to an impedance range of 370.21 to 766.08 jΩ. Using (3), this corresponds to an index ratio of approximately 1.6. The next step is to select a starting function for our pattern generation code which will produce a rotationally symmetric array of cells that vary smoothly from 3 mm in the center to 1 mm at the edges.

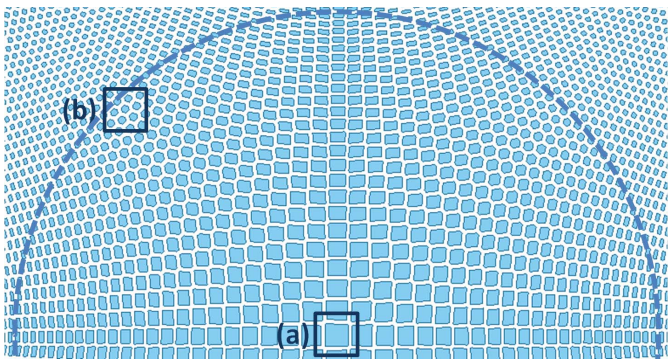

Fig. 10. Luneburg lens pattern used in the simulations. (only half shown) (a) Patches at the center of the lens measured 3 mm. (b) Patches at the edge of the lens measured 1 mm. These produce a 1.6:1 index ratio.

B. Patterns by Point Shifting Method and Simulation Results

We do not have a direct method to produce an arbitrary impedance function. Instead, we begin with a function that has the appropriate properties for our intended application, and then fit that function to produce the range of cell sizes that correspond to the desired impedance range. For example, a planar Luneburg lens requires a function with circular symmetry, and a local maximum in the center. The Luneburg lens pattern was generated by the point shifting method on a 93×93 point array with a starting function f

$$f = \sqrt{1000e^{-0.2(x^2+y^2)^{0.9}}}. \tag{4}$$

This function was chosen empirically to generate a smoothly varying pattern of cells with rotational symmetry to approximate the Luneburg lens function. A section of the lens, and details of the unit cells from the center and edge are shown in Fig. 10. As shown in Fig. 9, the range of patch sizes varies from 1 to 3 mm from the edge to the center of the lens, and these sizes were chosen to provide an index ratio of 1.4 as required for the Luneberg lens profile. The substrate is the same 2.5 mm thick Rogers 6010 as used in the unit cell analysis. The diameter of the lens is approximately 90 mm and the whole pattern dimensions are 140×140 mm. The pattern consists of 8281 PEC patches and there are 0.5 mm gaps between the cells.

This lens differs from the true Luneburg lens profile in several ways. First, it does not match the function in (1) exactly, it is only an approximation. Second, it does not have a distinct edge, as the cells simply get smaller away from the center at a rate that exponentially approaches the background cell size of approximately 1 mm. Nonetheless, we can define an approximate edge to roughly match the edge of the Luneburg lens function. Third, the cells end about 2 cm past the edge of the lens, and the surrounding material is dielectric clad ground plane, with an impedance of 75.5 jΩ [25]. In spite of these differences, this approach has the advantage that the index varies smoothly, aside from the

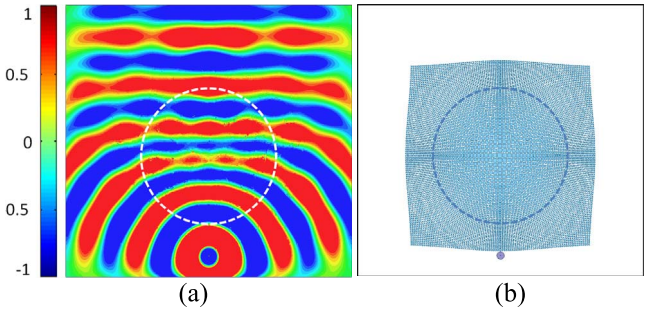

Fig. 11. (a) Normalized electric field at 7.5 GHz. Simulated data showing the field of a collimated surface wave produced from a monopole feed. (b) Area of the lens and surrounding board. The edge of the lens is approximate because it does not have a distinct boundary.

discrete nature of the cells, and we do not need to use shells or rings as in some other planar lens structures [26].

Furthermore, we do not need to match (1) exactly to obtain a structure with measurable lensing effects. Note that the purpose of this paper is not to build a planar Luneburg lens—that has been done many times before. The purpose is to introduce a new patterning technique for producing smoothly varying artificial impedance surfaces. The lens is just an example of a simple, well-known function with practical applications. We include it here to validate that our patterning method can produce structures with predictable and measurable properties.

The Luneburg lens pattern was simulated using the driven modal solver in Ansys HFSS. Fig. 11 shows the field plot at 2 mm above the board at 7.5 GHz. There is a coaxial feed in front of the pattern which generates circular waves that propagate over the lens pattern. The wavefronts are flattened as they pass through the lens pattern. As shown in this figure, the printed impedance surface produces a collimated beam at the output of the lens, as expected, validating our patterning procedure.

IV. Beam Shifting Patterning

In addition to the lens, we have also studied a structure that explicitly requires anisotropy, to demonstrate the usefulness of this structure for generating anisotropic patterns. As an example, we have designed a beam shifting structure. Such structures have been designed previously using anisotropic metasurfaces [3]. However, previous work involved homogeneous impedance surfaces because of the difficulty of patterning inhomogeneous anisotropic surfaces.

The beam shifter can be understood by considering that waves in an anisotropic medium will refract toward the lower index direction [27]. By gradually tilting the direction of low impedance, the wave can be made to follow a desired path.

The beam shifting pattern was generated with starting function f

$$f = \frac{x}{2} - 2\mathrm{Sin}(5x + y). \tag{5}$$

The patterning method resulted in 1154 PEC patches which were printed on a grounded 2.5 mm thick Rogers 6010 substrate. The size of the entire structure is 56 mm × 88 mm.

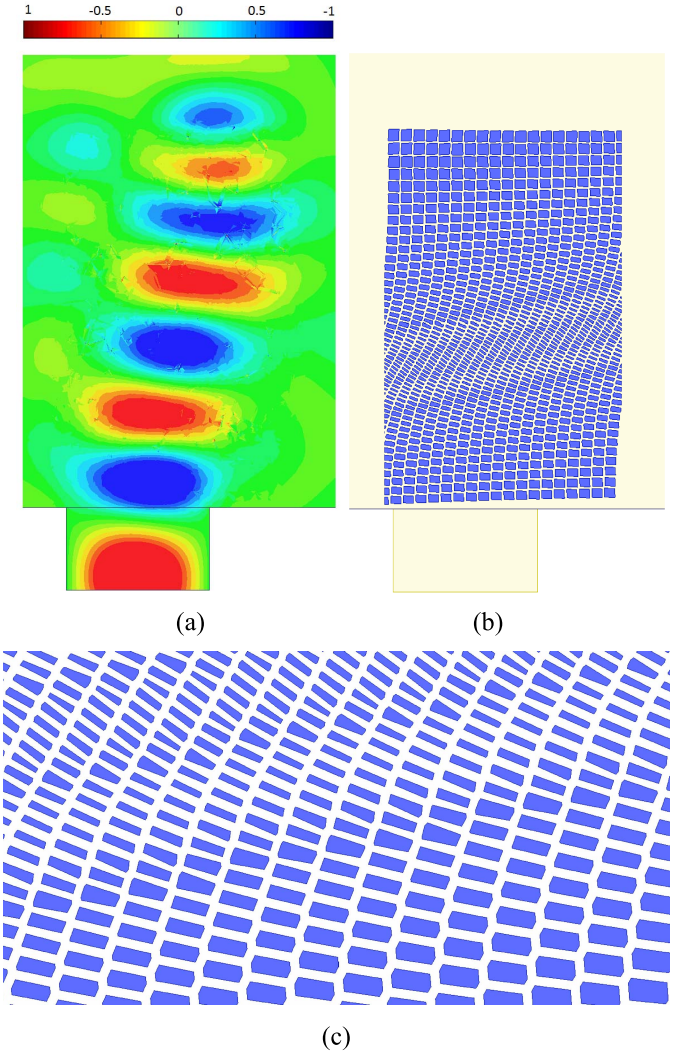

Fig. 12. (a) Normalized electric field at 7 GHz. (b) Pattern on the board with a wave guide source. (c) Enlarged section of the beam shifting surface.

For the elongated patches near the center of the beam shifting structure, the impedance was 260 jΩ in the low direction and 374 jΩ in the high direction. Simulations, shown in Fig. 12, indicate that a beam excited at one end of the structure (such as generated by a waveguide aperture) will be shifted by nearly an entire beamwidth at the other end of the structure. This smoothly varying beam shifting structure represents a pattern that would be impossible to produce using existing techniques. The performance of both the Luneburg lens and the beam shifting surface were verified experimentally, as described in the following section.

V. Experiments

The Luneburg lens pattern was fabricated using printed circuit fabrication technology, and is shown in Fig. 13. The panel is 190 × 180 mm with 8281 copper patches on top of the board, and bottom of the board is a ground. There is a 5 mm diameter hole in front of the pattern for a coaxial feed which is the excitation source. A vertical probe was swept 2 mm above the surface along a 1 mm grid and an Agilent E5071C vector network analyzer recorded the magnitude and

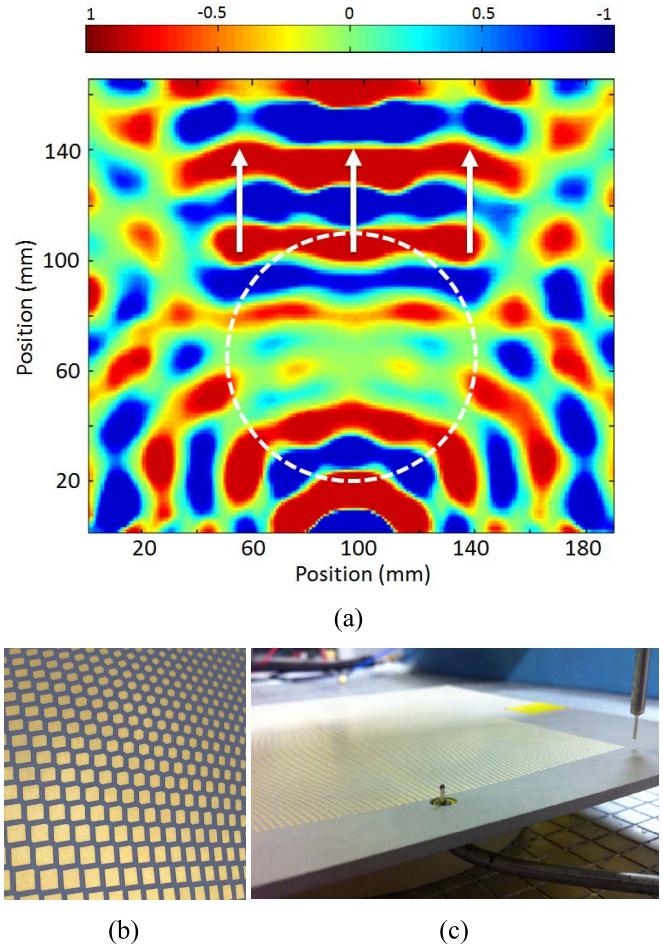

Fig. 13. (a) Normalized near field plot of the surface waves scanned over a 190 × 165 mm area, indicating the collimating capabilities of the lens. The scan starts just beyond the feed point. (b) Closeup photo of the fabricated Luneburg lens pattern. (c) Details of the feed and the measurement technique, including the probe visible at one extreme of the scan region.

the phase of the surface wave. Normalized field results are shown in Fig. 13(a). The circular wavefronts generated by the feed are transformed into flat wavefronts at the opposite side of the lens, as expected. The essential characteristics of the pattern match that shown in Fig. 11, verifying that our technique produces practical impedance surface patterns that match simulation results, and perform a useful function of collimating surface waves. The flat wavefronts emerging from the surface of the lens opposite to the feed are the expected behavior for a Luneburg lens. The additional variations along the edges of the measurement area are artifacts that are indicative of a standing wave pattern which is likely caused by reflections from the edges of the board.

The beam shifting structure was excited by a WR137 waveguide placed adjacent to the surface at one edge. A field map was produced in the same way as for the lens described above, and is plotted in Fig. 14. The beam center is smoothly shifted from 50 to 70 mm along the length of the structure. Note also that the phase fronts begin and end parallel to the front and back edges of the surface, gradually tilt to the right in the central region, following the anisotropic impedance pattern.

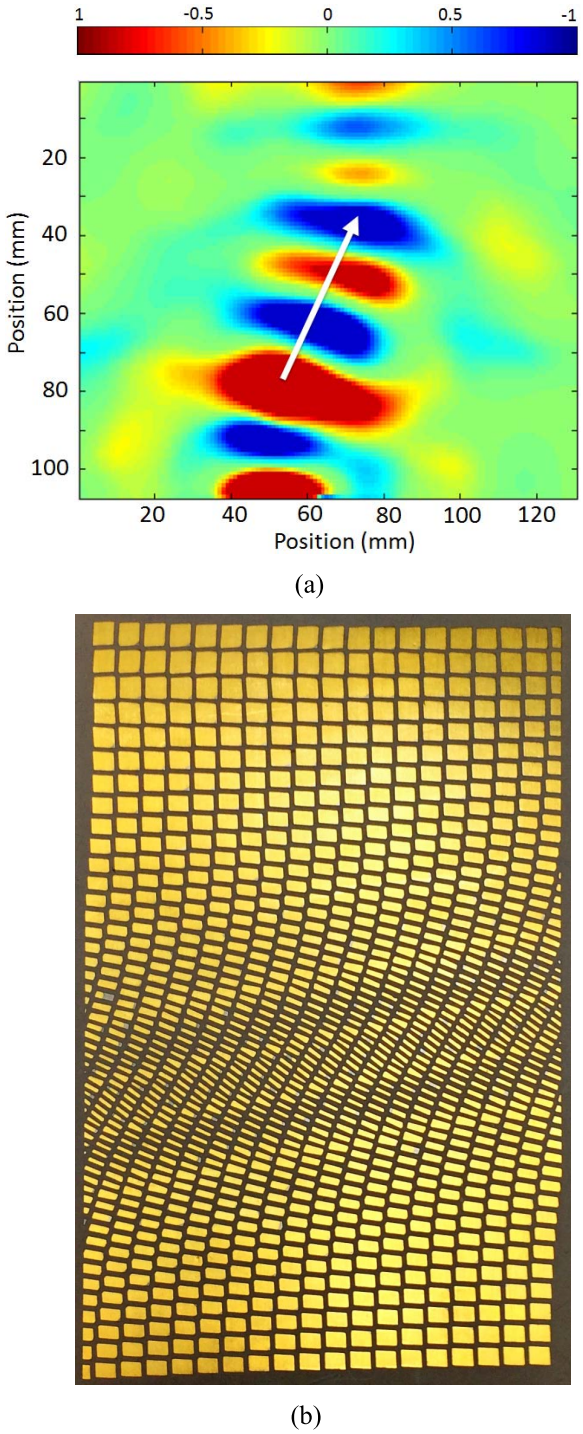

Fig. 14. (a) Normalized near field plot of the surface waves scanned over a 130 × 07 mm area. The arrow represents waves propagating direction to the tilted angle. (b) Fabricated beam shifting pattern.

VI. Conclusion

We have introduced a patterning technique for generating arbitrary impedance surfaces. It provides several advantages over other patterning approaches such as the ability to produce a range of cell sizes, shapes, and orientations, including smoothly varying and highly anisotropic impedance surfaces. Specifically, the ability to produce smoothly varying impedance surfaces with reduced symmetry cells, which are

important for achieving high anisotropy, has been absent from all previous patterning methods. We have illustrated the limitations of existing techniques, as well as other potential approaches such as conformal mapping, and path-dependent methods. We have shown that our technique based on point shifting with Voronoi cell generation can produce impedance surfaces with a wide range of useful properties. We have chosen a simple and practical example to validate our method experimentally, in the form of a planar Luneburg lens as well as an anisotropic beam shifting structure.

We expect that this method will be used to design a wide range of future impedance surface for applications such as planar antennas, scattering control, and interference mitigation. However, there are also several fundamental questions that are topics for future research. First, the starting function is currently chosen empirically to produce a described range of predetermined cell geometries. We need a method to translate the desired impedance function directly to the starting function. Second, the limitations of this method are not known, such as the range of impedance functions that are achievable. Third, aside from certain special cases such as the lens illustrated here, it is not known what impedance function is required to produce a specific surface wave or scattering response. Addressing these issues will allow us to use the method described here to produce arbitrary impedance surfaces for a wide range of applications.

ACKNOWLEDGMENT

The authors would like to thank R. Quarfoth, the researcher at HRL Laboratories for valuable suggestions and contributions during the work.

REFERENCES

[1] R. G. Quarfoth and D. F. Sievenpiper, "Nonscattering waveguides based on tensor impedance surfaces," *IEEE Trans. Antennas Propag.*, vol. 63, no. 4, pp. 1746–1755, Apr. 2015.

[2] A. M. Patel and A. Grbic, "Transformation electromagnetics devices based on printed-circuit tensor impedance surfaces," *IEEE Trans. Microw. Theory Techn.*, vol. 62, no. 5, pp. 1102–1111, May 2014.

[3] R. Quarfoth and D. Sievenpiper, "Surface wave scattering reduction using beam shifters," *IEEE Antennas Wireless Propag. Lett.*, vol. 13, pp. 963–966, 2014.

[4] D. Sievenpiper, J. Colburn, B. Fong, J. Ottusch, and J. Visher, "Holographic artificial impedance surfaces for conformal antennas," in *Proc. IEEE Antennas Propag. Soc. Int. Symp.*, vol. 1B. Jul. 2005, pp. 256–259.

[5] R. Quarfoth and D. Sievenpiper, "Artificial tensor impedance surface waveguides," *IEEE Trans. Antennas Propag.*, vol. 61, no. 7, pp. 3597–3606, Jul. 2013.

[6] C. L. Holloway, E. F. Kuester, J. A. Gordon, J. O'Hara, J. Booth, and D. R. Smith, "An overview of the theory and applications of metasurfaces: The two-dimensional equivalents of metamaterials," *IEEE Antennas Propag. Mag.*, vol. 54, no. 2, pp. 10–35, Apr. 2012.

[7] C. L. Holloway, D. C. Love, E. F. Kuester, J. A. Gordon, and D. A. Hill, "Use of generalized sheet transition conditions to model guided waves on metasurfaces/metafilms," *IEEE Trans. Antennas Propag.*, vol. 60, no. 11, pp. 5173–5186, Nov. 2012.

[8] D. Sievenpiper, L. Zhang, R. F. J. Broas, N. G. Alexopolous, and E. Yablonovitch, "High-impedance electromagnetic surfaces with a forbidden frequency band," *IEEE Trans. Microw. Theory Techn.*, vol. 47, no. 11, pp. 2059–2074, Nov. 1999.

[9] B. H. Fong, J. S. Colburn, J. J. Ottusch, J. L. Visher, and D. F. Sievenpiper, "Scalar and tensor holographic artificial impedance surfaces," *IEEE Trans. Antennas Propag.*, vol. 58, no. 10, pp. 3212–3221, Oct. 2010.

[10] G. Minatti *et al.*, "Modulated metasurface antennas for space: Synthesis, analysis and realizations," *IEEE Trans. Antennas Propag.*, vol. 63, no. 4, pp. 1288–1300, Apr. 2015.

[11] C. Pfeiffer and A. Grbic, "Planar lens antennas of subwavelength thickness: Collimating leaky-waves with metasurfaces," *IEEE Trans. Antennas Propag.*, vol. 63, no. 7, pp. 3248–3253, Jul. 2015.

[12] L. V. Ahlfors, *Conformal Invariants: Topics in Geometric Function Theory*, vol. 371. Providence, RI, USA: AMS, 2010.

[13] U. Leonhardt, "Optical conformal mapping," *Science*, vol. 312, no. 5781, pp. 1777–1780, 2006.

[14] H. Chen, C. T. Chan, and P. Sheng, "Transformation optics and metamaterials," *Nature Mater.*, vol. 9, pp. 387–396, May 2010.

[15] S. H. Lo, "A new mesh generation scheme for arbitrary planar domains," *Int. J. Numer. Methods Eng.*, vol. 21, no. 8, pp. 1403–1426, 1985.

[16] R. K. Luneburg and M. Herzberger, *Mathematical Theory of Optics*. Berkeley, CA, USA: Univ. of California Press, 1964.

[17] G. Peeler and H. Coleman, "Microwave stepped-index Luneberg lenses," *IRE Trans. Antennas Propag.*, vol. 6, no. 2, pp. 202–207, Apr. 1958.

[18] G. Peeler and D. Archer, "A two-dimensional microwave Luneberg lens," *Trans. IRE Prof. Group Antennas Propag.*, vol. 1, no. 1, pp. 12–23, Jul. 1953.

[19] M. de Berg, M. van Kreveld, M. Overmars, and O. C. Schwarzkopf, *Computational Geometry*. Berlin, Germany: Springer-Verlag, 2000.

[20] L. Brillouin, *Wave Propagation in Periodic Structures: Electric Filters and Crystal Lattices*. North Chelmsford, MA, USA: Courier Corporation, 2003.

[21] C. Pfeiffer and A. Grbic, "A printed, broadband Luneburg lens antenna," *IEEE Trans. Antennas Propag.*, vol. 58, no. 9, pp. 3055–3059, Sep. 2010.

[22] K. Sato and H. Ujiie, "A plate Luneberg lens with the permittivity distribution controlled by hole density," *Electron. Commun. Jpn. I, Commun.*, vol. 85, no. 9, pp. 1–12, 2002.

[23] R. Quarfoth and D. Sievenpiper, "Broadband unit-cell design for highly anisotropic impedance surfaces," *IEEE Trans. Antennas Propag.*, vol. 62, no. 8, pp. 4143–4152, Aug. 2014.

[24] R. Quarfoth and D. Sievenpiper, "Anisotropic surface impedance cloak," in *Proc. IEEE Antennas Propag. Soc. Int. Symp. (APSURSI)*, Jul. 2012, pp. 1–2.

[25] R. E. Collin, *Field Theory of Guided Waves*. Hoboken, NJ, USA: Wiley, 1991.

[26] M. Huang, S. Yang, F. Gao, R. Quarfoth, and D. Sievenpiper, "A 2-D multibeam half Maxwell fish-eye lens antenna using high impedance surfaces," *IEEE Antennas Wireless Propag. Lett.*, vol. 13, pp. 365–368, 2014.

[27] D. J. Gregoire and A. V. Kabakian, "Surface-wave waveguides," *IEEE Antennas Wireless Propag. Lett.*, vol. 10, pp. 1512–1515, 2011.

Jiyeon Lee (S'14) received the B.S. degree from Hongik University, Seoul, South Korea, in 2007, and the M.S. degree from the University of California at San Diego, San Diego, CA, USA, in 2013, where she is currently pursuing the Ph.D. degree.

From 2008 to 2011, she was a Software Engineer of Management Information System at SK C&C, Seoul. Her current research interests include artificial impedance surfaces, metamaterials, antenna, and communication circuits.

Daniel F. Sievenpiper (M'94–SM'04–F'09) received the B.S. and Ph.D. degrees in electrical engineering from the University of California at Los Angeles, Los Angeles, CA, USA, in 1994 and 1999, respectively.

He was the Director of the Applied Electromagnetics Laboratory at HRL Laboratories, LLC., Malibu, CA, USA, where his research included artificial impedance surfaces, conformal antennas, tunable and wearable antennas, and beam steering methods. He is currently a Professor with the University of California at San Diego, San Diego, CA, USA. He has more than 70 issued patents and more than 100 technical publications. His current research interests include antennas and electromagnetic structures.

Prof. Sievenpiper was a recipient of the URSI Issac Koga Gold Medal in 2008. Since 2010, he has been an Associate Editor of the IEEE ANTENNAS AND WIRELESS PROPAGATION LETTERS.